New magnetic phenomena in $TbNi_2$

1999 J. Phys.: Condens. Matter 11 7893

(http://iopscience.iop.org/0953-8984/11/40/314)

J. Phys.: Condens. Matter **11** (1999) 7893–7905. Printed in the UK PII: S0953-8984(99)04402-1

New magnetic phenomena in $TbNi_2$

E Gratz†¶, E Goremychkin‡, M Latroche§, G Hilscher†, M Rotter†, H Müller†, A Lindbaum†, H Michor†, V Paul-Boncour§ and T Fernandez-Diaz‖

† Institut für Experimentalphysik, Vienna University of Technology, Wiedner Hauptstrasse 8–10, A-1040 Vienna, Austria
‡ Argonne National Laboratory, Argonne, IL 60439, USA
§ CNRS–LCMTR–UPR 209, 94320 Thiais Cédex, France
‖ ILL, Grenoble, France

E-mail: gratz@xphys.tuwien.ac.at

Received 19 May 1999

Abstract. Structural investigations at room temperature revealed that $TbNi_2$ does not crystallize in the Laves phase structure, but shows a superstructure of the Laves phase with the space group F-43m. Susceptibility, specific heat, magnetostriction and magnetoresistance measurements on polycrystalline specimens showed an additional magnetic phase transition at $T_R = 14$ K below the Curie temperature of $T_C = 36 \pm 0.2$ K. In order to clarify the nature of this magnetic phase transition at 14 K, elastic neutron diffraction below and above T_R and T_C was performed. The analysis of these data showed that this transition at T_R is due to the rotation of the Tb moments on three of the total of eight non-equivalent Tb sites in the rhombohedrally distorted unit cell in the magnetic ordered state. This rotation of these Tb moments is out of the [111] direction into a plane perpendicular to the space diagonal. The cause for this magnetic instability is due to an interplay of the regularly arranged vacancies in the superstructure and the crystal field level position which has been studied by inelastic neutron scattering.

1. Introduction

Rare earth–nickel Laves phase compounds (RNi_2) were the subject of extensive investigations in the past decades because of their relatively simple crystal structure and the commonly accepted assumption that Ni carries no moment, in contrast to the other RT_2 compounds with T = Mn, Fe and Co where there are either intrinsic moments (i.e. RFe_2) or induced moments (RCo_2) on the T sites.

First magnetic structure investigations of $TbNi_2$ using the neutron diffraction technique were performed by Felcher *et al* [1]. These authors reported that $TbNi_2$ crystallizes in the cubic Laves phase structure and ferromagnetic lines as well as additional peaks appear in the diffraction pattern at 4.2 K, but the magnetic scattering is rather sensitive to sample preparation. Furthermore, they realized that the intensity of the nuclear lines were not in satisfactory agreement with the calculated ones, however, under the assumption that 6% of the rare earth sites are not occupied by Tb a reasonable fit could be obtained. About 30 years after this finding, Latroche *et al* [2, 3] showed that $TbNi_2$ as well as most of the other RNi_2 compounds crystallizes in a cubic structure with regularly arranged vacancies on the rare earth sites which is a superstructure (space group F-43m) of the cubic Laves phase with cell parameters twice as

¶ Corresponding author.

large as the lattice parameter given for the RNi_2 Laves phase. Single phase samples with this superstructure of the cubic Laves phase can, only be obtained in a R deficient composition. The formation of a superstructure with ordered vacancies at the R sites is energetically favourable; this has been confirmed by *ab initio* total energy calculations [4]. Samples prepared with the exact 1:2 stoichiometry frequently show the orthorhombic RNi compound as impurity phase. The most suitable composition for the Tb–Ni compound is $Tb_{0.96}Ni_2$ [3]. Recent investigations on some of the $R_{1-x}Ni_2$ compounds (R = Y, Sm, Gd, Tb) with x near 0.05 showed that in all of them structural order–disorder transitions (from the superstructure (F-43m) into the cubic Laves phase ($Fd3m$)) at temperatures far above room temperature occur ($Y_{1-x}Ni_2$ (740 K), $Sm_{1-x}Ni_2$ (550 K), $Gd_{1-x}Ni_2$ (600 K) and $Tb_{1-x}Ni_2$ (450 K) [5]). Pressure experiments using synchrotron radiation and a diamond pressure cell revealed that these transitions can be lowered down to room temperature with pressure in the range of about 15–20 GPa [5].

The aim of the present work was to re-investigate the magnetic properties of the $TbNi_2$ compound, since we are now able to synthesize $TbNi_2$ of very high quality, however not in the cubic Laves structure but with the superstructure. For simplicity, we are still using the notation $TbNi_2$ instead of $Tb_{0.96}Ni_2$ (or $Tb_{0.98}Ni_2$, see below) for the compound under consideration.

2. Sample preparation and experimental details

Polycrystalline samples used for the present investigations were prepared by induction melting under a protective argon atmosphere in a water cooled copper crucible. In order to investigate the influence of the stoichiometry and the annealing conditions on the sample purity we prepared two kinds of sample, one with the stoichiometry 0.96:2 and the other with the 1:2 stoichiometry. Parts of both batches have been annealed either at 650 °C for one month or at 1200 °C for 15 h. It has been found that both annealing conditions give comparable results; however the stoichiometry 1:2 led to the appearance of the Tb-richer 1:1 (TbNi) phase as an impurity phase. Independent of the annealing procedure and the stoichiometry the main phase always forms the superstructure but not the Laves phase. The phase purity was checked by metallography, electron microprobe analysis and density measurements. The x-ray powder pattern was indexed in the F-43m space group revealing a cell parameter of $a = 14.3422(6)$ Å at 295 K. Neutron diffraction experiments were performed on a sample material with the nominal composition 0.98:2 (determined by electron microprobe analysis) on the D1A diffractometer at ILL in Grenoble. The wavelength used was 1.91 Å and the step-width for recording the pattern was 0.05° (in 2Θ). The grain size of the powder was smaller than 50μm. The powdered specimen with a weight of about 15 g was encapsulated in a cylindrical sample holder of 8 mm diameter under N_2 atmosphere. Diffraction patterns have been recorded from $2\Theta = 10$ up to 150 degrees at 1.5, 10, 27, 33, 37 and 50 K. The data were corrected for absorption and evaluated by the FULLPROF program package [6]. For the study of the crystal field properties the time of flight chopper spectrometer LRMECS at the spallation neutron source at Argonne National Laboratory (USA) has been used with incident neutron energies of 15 and 25 meV. For the characterization of the bulk properties of $TbNi_2$ the following measuring techniques under the following conditions have been applied. The electrical resistivity was measured using a standard four probe technique in fields up to 1 T. Specific heat measurements in external fields were carried out in a quasi-adiabatic calorimeter employing a modified Nernst step-heating technique. AC susceptibility and DC magnetization measurements were performed with a calibrated AC susceptometer (80 Hz and field amplitude of 200 A m^{-1}) and a SQUID magnetometer in fields up to 6 T, respectively. The thermal expansion and the magnetostriction were measured by a capacitance dilatometer in the temperature range from 4 up to 50 K and in various external fields up to 1 T.

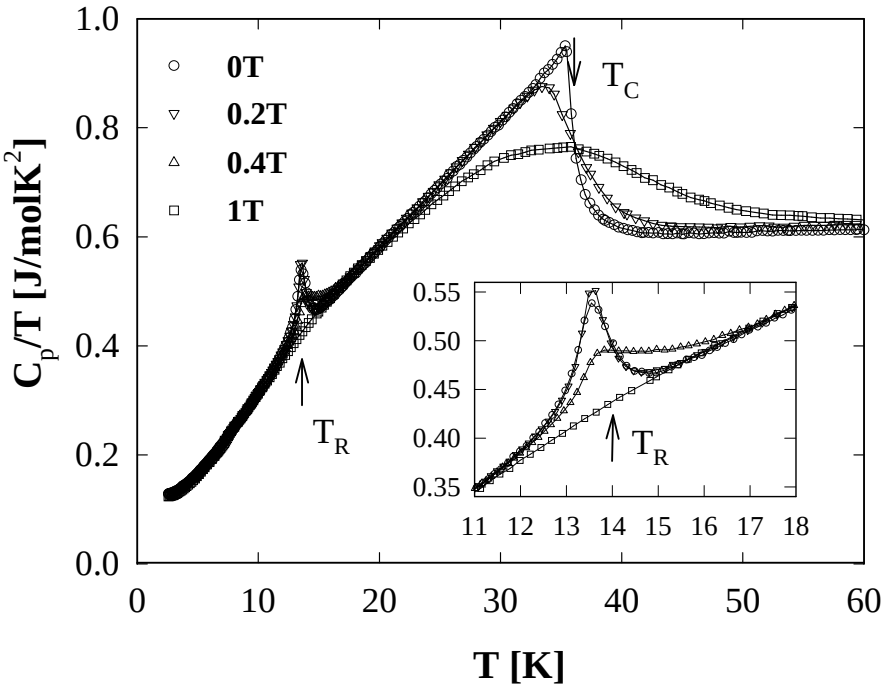

Figure 1. The temperature dependence of the specific heat (C_P/T) of $TbNi_2$ at various magnetic fields is depicted: T_C denotes the Curie temperature ($=36 \pm 0.2$ K); the anomaly at $\approx$14 K (T_R) is caused by a change of the magnetic structure (spin reorientation). The inset shows the suppression of the spin reorientation with increasing magnetic fields.

3. Experimental results and discussion

From the temperature variation of the specific heat, $C_P(T)$, and the coefficient of the thermal expansion, $\alpha(T)$, shown in figures 1 and 2 we determined the onset of long range magnetic order of $TbNi_2$ (the exact stoichiometry of the sample material used was $Tb_{0.96}Ni_2$) at 36 ± 0.2 K (T_C) taking the inflection point in $C_P(T)$ and $\alpha(T)$ as a value for T_C. Furthermore both $C_P(T)$ and $\alpha(T)$ revealed the existence of an anomaly within the magnetically ordered state at about 14 K (T_R) which has not been mentioned before in any of the previous publications (see table 3). Measurements of the electrical resistivity with and without a magnetic field confirmed the existence of this anomaly, although the small step-like increase in $\rho(T)$ at zero field appears at slightly higher temperature ($\sim$17 K) (see figure 3). The hump at T_C in ρ against T and its fast disappearance with increasing fields indicate the existence of enhanced short range correlations among the Tb moments around T_C (see e.g. the review by Gratz and Zuckermann [7] and references therein). The magnetoresistance $(\rho - \rho_0)/\rho_0$ ($=\Delta\rho/\rho_0$) in a field of 2T is given in the inset of figure 3. The minimum in $\Delta\rho/\rho_0$ at T_C is characteristic for a ferromagnetic transition. In fields higher than about 1 T there is no further increase of the minimum depth, since the fluctuations are already suppressed by such an external field. These bulk measurements are completed by AC susceptibility (figure 4) and DC magnetization measurements (figure 5). The anomaly at 14 K can, however, be resolved only by the former technique (χ'). This, together with the finding that the anomaly can be suppressed with external fields as low as 1 T (see specific heat and thermal expansion) and that no significant losses

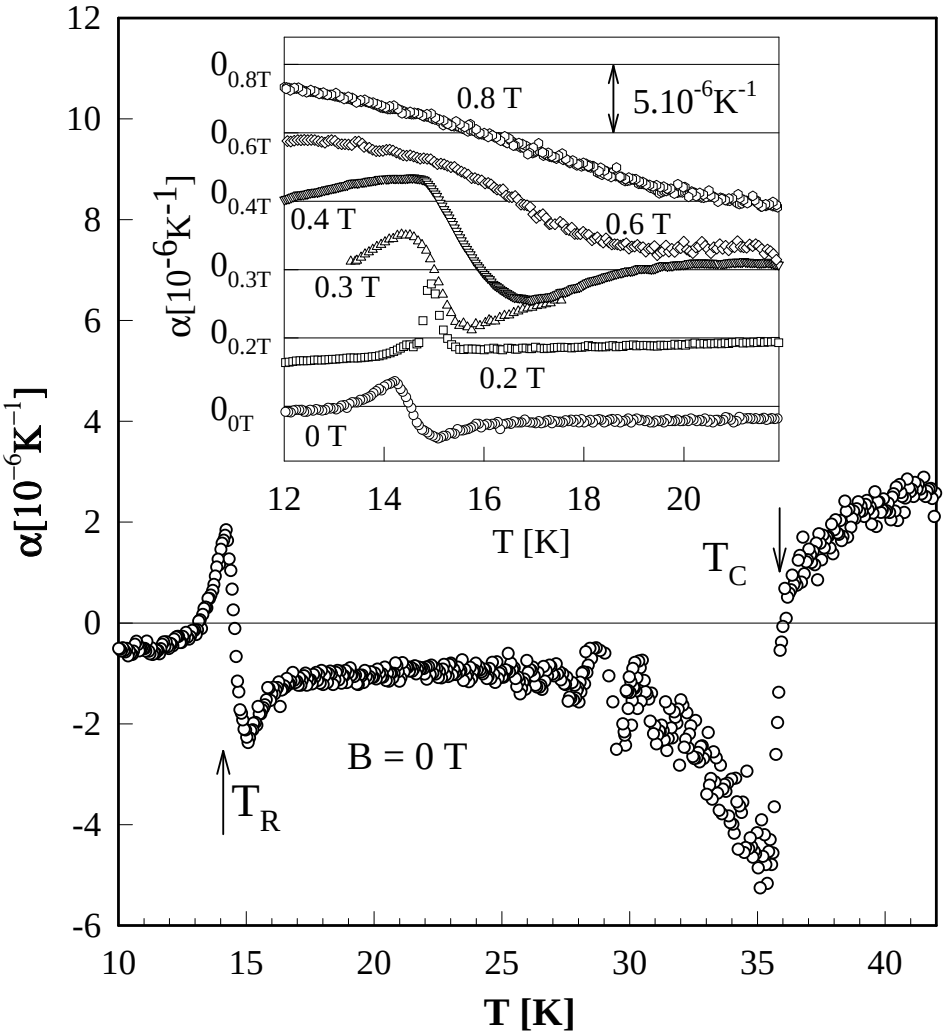

Figure 2. The temperature dependence of the coefficient of the thermal expansion (α) is shown. The inset shows the temperature variation of the magnetostriction (thermal expansion in external magnetic fields) in the vicinity of the spin reorientation temperature in fields up to 0.8 T.

(associated with a finite imaginary susceptibility χ'') occur at about T_R compared to those at T_C in the AC susceptibility measurement indicate that a reversible spin reorientation occurs at this temperature T_R. These magnetization data will be discussed below in more detail.

In order to determine the magnetic structure of $TbNi_2$ above and below T_R and thus the nature of the anomaly associated with T_R, neutron diffraction measurements were performed. The diffraction pattern at 50 K is in accordance with those obtained from the x-ray diffraction at room temperature; both patterns could correctly be refined in the cubic superstructure with the space group F-43m with a cell parameter $a = 14.292$ Å at 50 K ($a = 14.3422(6)$ Å at room temperature).

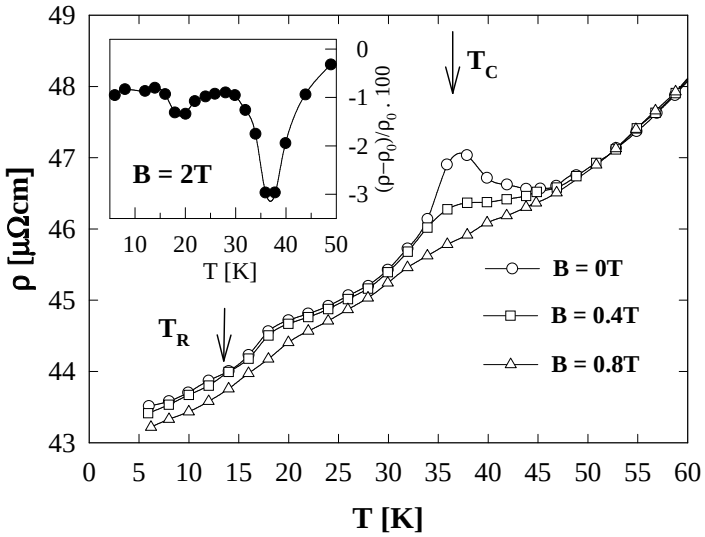

Figure 3. The temperature dependence of the electrical resistivity in the low temperature region in different external magnetic fields is shown. The inset shows the temperature variation of the magnetoresistance at 2 T.

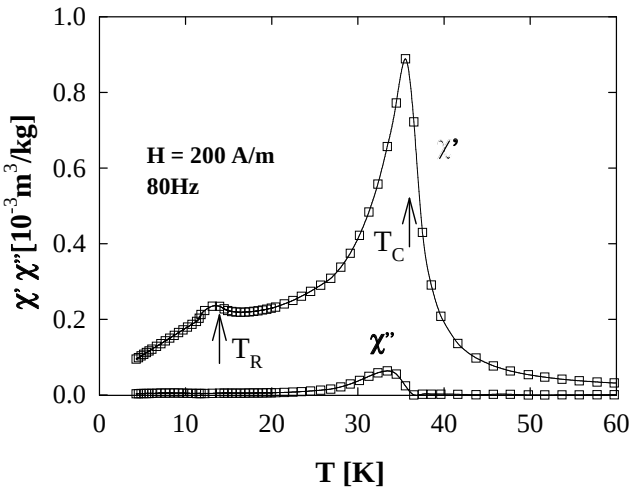

Figure 4. AC susceptibility as a function of temperature is given. χ' and χ'' denote the real and the imaginary part of the susceptibility at 80 Hz and $H = 200$ A m^{-1}.

3.1. Magnetic structure at $T_R < T < T_C$

The neutron pattern at 37, 33 and 27 K can still be indexed in the cubic superstructure, but there is an increasing magnetic intensity superimposed on the Bragg reflections due to the ferromagnetic alignment of Tb moments along the [111] direction. The fit procedure for 27, 33 and 37 K reveals that all the Tb moments are uniformly aligned along [111] (irrespective of whether the structure is considered as cubic (F-43m) or the increasing rhombohedral distortion is taken into account (see below)).

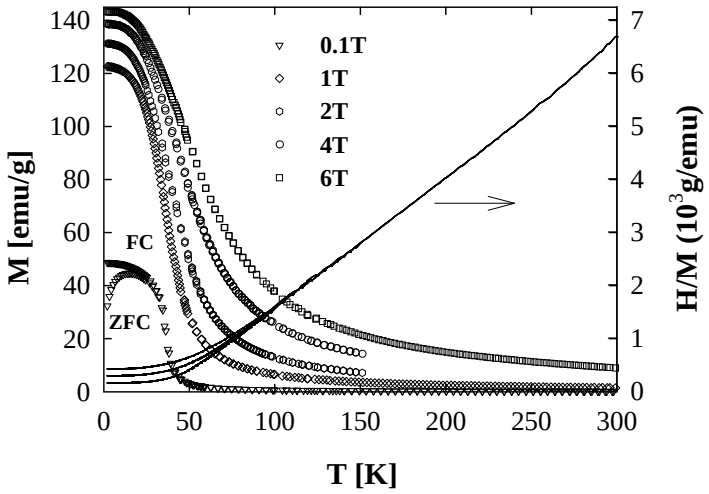

Figure 5. The magnetization at different fields as labelled (symbols) and the inverse susceptibility at 0.1, 1 and 2 T (lines) as a function of temperature is shown.

To clarify the nature of the magnetic phase transition at T_R the magnetic structure below T_R has to be determined, including also the distortion of the superstructure unit cell, which cannot be ignored at the lowest temperatures in particular for the analysis of the data at 1.5 K. A distortion of the cubic unit cell along the space diagonal (i.e. rhombohedral distortion) is plausible because of the magneto-elastic coupling of the Tb moments, pointing in the [111] direction to the lattice. In order to determine the temperature variation of the distortion as precisely as possible selected lines of the neutron pattern have been investigated separately using a single line analysis. For these analyses the reflections with the Miller indices: (800), (880), (844) and (888) (in the cubic description) were selected. Because of the smallness of the absolute value of the rhombohedral distortion, in particular just below T_C (for the patterns at 33 and 27 K), the measured intensity has been fitted with only one line shape function and the increasing half-width (FWHM) of this function has been taken as a measure for the temperature variation of the distortion. Both the (880) and the (844) Bragg reflection show a broadening (which means splitting) due to the rhombohedral distortion, whereas there is no broadening for the (800) Bragg reflection observable (which should not be split in a rhombohedrally distorted cubic cell). For the (888) Bragg reflection ($2\Theta \approx 135.5^\circ$) splitting into two lines with the intensity ratio 1:3 and a separation of about 0.4° could be determined at 1.5 K. Using a hexagonal description of the rhombohedrally distorted superstructure unit cell these lines are indexed with the (0 0 24) and the (808) Miller indices. A quantitative determination of the distortion using the following equation for the distortion parameter:

$$\lambda_{111} = \frac{2}{3}\frac{(c_h/\sqrt{3}) - a_h\sqrt{2}}{a_h\sqrt{2}}$$

yields $\lambda_{111} = 1.4 \times 10^{-3}$. The positive sign of λ_{111} means that the cell is stretched along [111]. A rhombohedral distortion of the unit cell of $TbNi_2$ has already been discovered by Markosyan [8]: the magnitude of the distortion and its temperature dependence reported there are in good agreement with our data; however the sign is opposite. The latter is due to a misprint [9].

Table 1. The relation between the Tb sites in the cubic superstructure unit cell (space group F-43m) and the rhombohedrally distorted unit cell (space group $R3m$) in a hexagonal description is shown.

Cubic F-43m						Rhombohedral $R3m$ (hexagonal description)					
		x	y	z				x	y	z	
Tb1	4a	0	0	0		Tb1	3a	0	0	z	$z = 0.000$
Tb2	4b	1/2	1/2	1/2		Tb2	3a	0	0	z	$z = 0.494$
Tb3	16e	x	x	x	$x = 0.103$	Tb4	3a	0	0	z	$z = 0.099$
						Tb5	9b	x	$2x$	z	$x = 0.140$
											$z = 0.962$
Tb4	16e	x	x	x	$x = 0.630$	Tb3	3a	0	0	z	$z = 0.623$
						Tb6	9b	x	$2x$	z	$x = 0.836$
											$z = 0.788$
Tb5	24g	x	1/4	1/4	$x = 0.006$	Tb7	9b	x	$2x$	z	$x = 0.843$
											$z = 0.161$
						Tb8	9b	x	$2x$	z	$x = 0.826$
											$z = 0.658$

3.2. The magnetic structure at $1.5 \leqslant T \leqslant T_R$

In the rhombohedrally distorted superstructure unit cell (space group $R3m$) are eight non-equivalent Tb sites whereas there are only five non-equivalent sites in the undistorted superstructure cell. Table 1 shows the relation between the Tb sites in the cubic and in the rhombohedrally distorted unit cell (in the hexagonal description). The FULLPROF refinement revealed for the arrangement of the Tb moments that:

(i) The moments on five of the eight Tb sites (Tb2, Tb3, Tb6, Tb7, Tb8) are still aligned along the [111] direction.

(ii) The moments on the Tb4 and Tb5 sites (which are nearest to the partially occupied Tb1 sites) are lying in a plane perpendicular to the [111] direction, however the direction within this plane is uncertain.

The sizes of all these Tb moments are equal, namely 8.3 μ_B/Tb.

(iii) As far as the Tb1 sites are concerned the fit procedure seems to show that these sites are partially occupied with a reduced moment size and an alignment approximately perpendicular to the [111] direction.

In figure 6 the elastic neutron scattering pattern at 1.5 K is shown. The symbols give the experimental data and the line through the data points shows the goodness of the fit procedure assuming the non-collinear structure on the three Tb sites as discussed above. The Bragg R-factor was 4.22% and the magnetic R-factor 7.22%. For further details of the structural parameters see table 2.

The conclusion from these elastic neutron experiments reveals that the nature of the magnetic phase transition at 14 K consists in a rotation of the Tb moments on three of the eight non-equivalent Tb sites into a plane perpendicular to the [111] magnetization direction. The magnetization measurements will be discussed in the light of the results obtained from neutron diffraction. Although the spin reorientation at $T_R = 14$ K is clearly resolved in the AC susceptibility, no anomaly at T_R can be seen in the low field (0.1 T) $M(T)$ measurements (shown in figure 5 for various magnetic fields). For low fields up to about 0.1 T there is a considerable irreversibility between the zero field cooled (ZFC) and field cooled (FC) branch of the DC magnetization (see figure 5) being indicative of the anisotropy of the magnetization and associated small domain wall width.

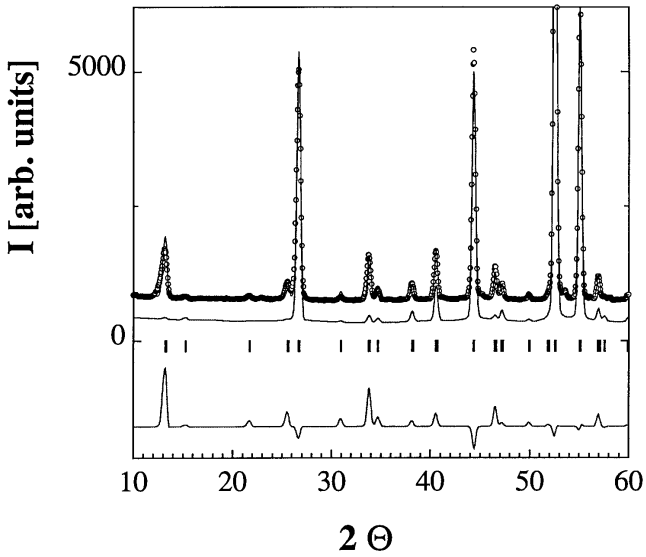

Figure 6. The symbols represent the neutron diffraction pattern at 1.5 K. The line through these data points corresponds to the Rietveld analysis using the FULLPROF program package for the non-collinear magnetic structure (details of this magnetic structure are given in table 2). The calculated pattern profile a little below the data points corresponds to the magnetic intensity for $T > T_R$, where all the Tb moments are aligned along [111]. The vertical bar pattern gives the positions of the magnetic intensities for the non-collinear magnetic structure. The lowest line in this figure shows the difference of calculated magnetic line intensity for the non-collinear minus the collinear structure.

The susceptibility (also shown in figure 5) is well described between 80 and 300 K by a modified Curie–Weiss law $\chi = \chi_0 + C/(T - \Theta)$ yielding $\chi_0 = 1.09 \times 10^{-8}$ emu g^{-1}, the paramagnetic Curie temperature $\Theta = 35$ K and an effective moment $\mu_{eff} = 9.55(3)\mu_B$ fu^{-1} which is slightly smaller than the theoretical value and indicates a crystal field influence. These values are in rough agreement with previous results collected in table 3.

According to the FULLPROF analysis discussed above one expects at low fields and low temperatures ($T < T_R$) a spontaneous moment of 5.8 μ_B fu^{-1} for a single crystal along the [111] axis, since only 33 of 47.25 Tb atoms per unit cell contribute with 8.3 μ_B along [111] to the bulk moment while the moment of the others are perpendicular (see table 2). Only an estimate of the spontaneous and 'low field' saturation magnetization can be obtained from the magnetization measurement of the polycrystalline samples at 2 K up to 6 T using an Arrott plot and a modified law of approach to saturation $M(H) = M_S(1 - A/H - B/H^2 + \chi H)$. Because of the suppression of the spin reorientation in external fields above about 1 T we included an additional term, χH, to account for the rotation of the magnetic moment into the direction of the external field. This yields 6.1 and 6.3 μ_B fu^{-1} ($Tb_{0.96}Ni_2$) for the spontaneous and 'low field' saturation magnetization, respectively. The slightly larger extrapolated values than that calculated from the neutron diffraction (5.8 μ_B fu^{-1}) can be attributed to the gradual suppression of the spin reorientation for fields larger than 0.2 T.

The overall shape of the magnetization and the heat capacity is typical for a mean field ferromagnet where the transition is washed out with growing fields and entropy is shifted to higher temperatures. The jump of the specific heat at T_C is only 70% of that expected ($\Delta C_p = 20.5$ J mol^{-1} K^{-1}) for a mean field ferromagnet with $J = 6$. The reduced gain

Table 2. A summary of the results of the FULLPROF refinement at 1.5 K for $TbNi_2$ (stoichiometry 0.98:2) is given. The columns show: The cell parameter a (=10.0956 Å)and c (=24.7800 Å) of the hexagonal unit cell, the position of the eight Tb and the ten Ni sites (x, y, z), the magnetic moments (M (μ_B)), the orientation of the Tb moments relative to the hexagonal c-axis (Θ) and within the plane perpendicular to the c-axis (φ) and the numbers of atoms on the different atomic sites.

$Tb_{0.98}Ni_2$ (1.5 K)			Space group $R3m$ (hexagonal descrip.)		Cell parameters: $a = 10.0956(1)$ Å $c = 24.7800(6)$ Å			
Atoms	x	y	z	B (Å^2)	M (μ_B)	φ (°)	θ (°)	N
Tb1	0	0	0	0.23(5)	6.97(49)	−103 (4)	−81 (2)	2.25
Tb2	0	0	0.494(3)		8.29 (5)	0	0	3
Tb3	0	0	0.623(3)			0	0	3
Tb4	0	0	0.099(3)			240	90	3
Tb5	0.140(1)	2x	0.962(3)			240	90	9
Tb6	0.836(1)	2x	0.788(3)			0	0	9
Tb7	0.843(1)	2x	0.161(3)			0	0	9
Tb8	0.826(1)	2x	0.658(3)			0	0	9
Ni1	0	0	0.305(3)	0.48(3)				3
Ni2	0	0	0.804(3)					3
Ni3	0.411(1)	2x	0.887(2)					9
Ni4	0.082(1)	2x	0.719(3)					9
Ni5	0.498(3)	2x	0.303(3)					9
Ni6	0.583(3)	2x	0.219(3)					9
Ni7	0.167(3)	2x	0.138(3)					9
Ni8	0.246(2)	2x	0.054(3)					9
Ni9	0.591(2)	0.928(2)	0.720(3)					18
Ni10	0.919(2)	0.576(2)	0.887(3)					18
	$R_{\omega p} = 6.54\%$				Bragg R-factor = 4.22%			
	$R_p = 4.76\%$				Magnetic R-factor = 7.22%			
	$R_{exp} = 1.28\%$							

Table 3. An overview of the magnetic bulk properties of $TbNi_2$ taken from the literature and the present work is shown. The last line shows the results obtained from the present investigation.

μ_s [μ_B fu^{-1}]	μ ($\mu_0 H$, T) [μ_B fu^{-1}]	T_c [K]	Θ [K]	μ_{eff} [μ_B fu^{-1}]	Reference
5.84		46			[10]
7.8[a]		45	35	9.82	[11]
	6.9 (2.6 T, 4 K)	35	44	9.71	[12]
	6.64 (2 T, 4 K)	37.5			[13]
		33			[14]
6.1[b]/6.3[c]	6.95 (6 T, 2 K)	36/14[d]	35	9.55	This work

[a] Extrapolated to infinite field.
[b] Spontaneous magnetization from an Arrott plot at 2 K.
[c] Low field saturation magnetization according to the modified law of approach to saturation (see text).
[d] Spin-reorientation temperature.

of entropy can be attributed to the influence of the crystal field and enhanced short range correlations in an extended temperature range above T_N.

The aim of crystal field study in the scope of this investigation was threefold: (i) To investigate whether the crystal field level scheme of our $TbNi_2$ compound with the

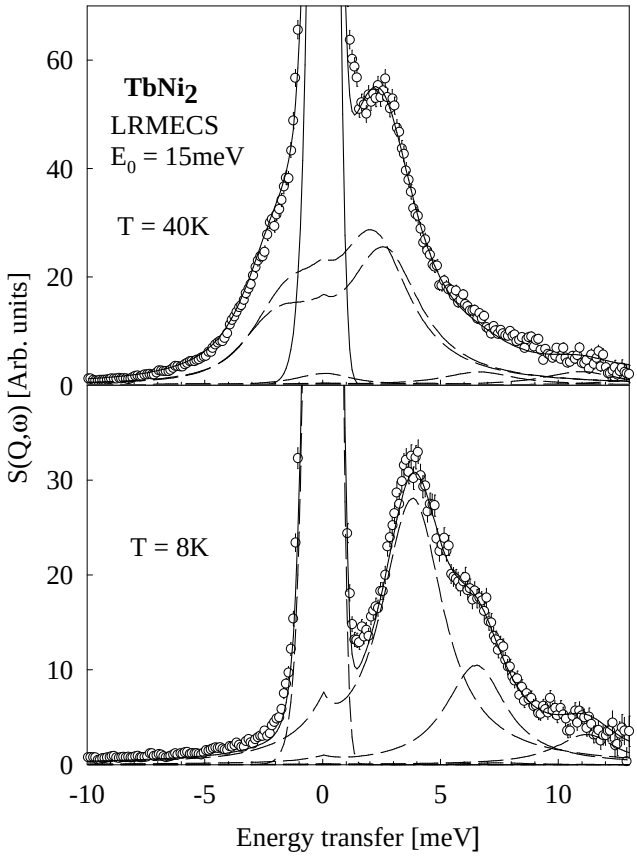

Figure 7. The inelastic neutron spectra (measured with LRMECS spectrometer at ANL) with an incident neutron energy of 15 meV in the paramagnetic state (40 K) and in the ordered state (8 K) is shown. The line through the data points represents the fit procedure described in the text.

superstructure is different from that by Goremychkin *et al* [17] for a $TbNi_2$ sample with the nominal 1:2 stoichiometry. (ii) To determine the influence of the crystal field on the temperature variation of the spontaneous magnetization. (iii) To study the role of the crystal field upon the magnetic phase transition at 14 K.

The inelastic neutron experiments were performed at the LRMECS instrument at ANL (Argonne) with incoming neutron energies of 15 and 25 meV. One spectrum was measured in the magnetically ordered state at 8 K and the other in the paramagnetic temperature region at 40 K. In figure 7 the inelastic neutron spectra (INS) for 15 meV incoming neutron energy (summed over scattering angles from 5° to 35°) in the paramagnetic and the ferromagnetic state are shown. The INS in the paramagnetic state is rather poor in structure (the pattern consists basically of one peak centred around 2.3 meV). It has been found that both experimental results, ours at 40 and at 8 K (shown in figure 7) and those of Goremychkin *et al* [17] at 80 and 10 K (see figure 6 there) are in good agreement. As will be shown below there is also a qualitative agreement in the level scheme and the corresponding wavefunction between ours and those of Goremychkin *et al* [17].

For the following quantitative analysis of the crystal field data it is important to note that we have made two simplifications: (i) we ignored the fact that $TbNi_2$ crystallizes in the

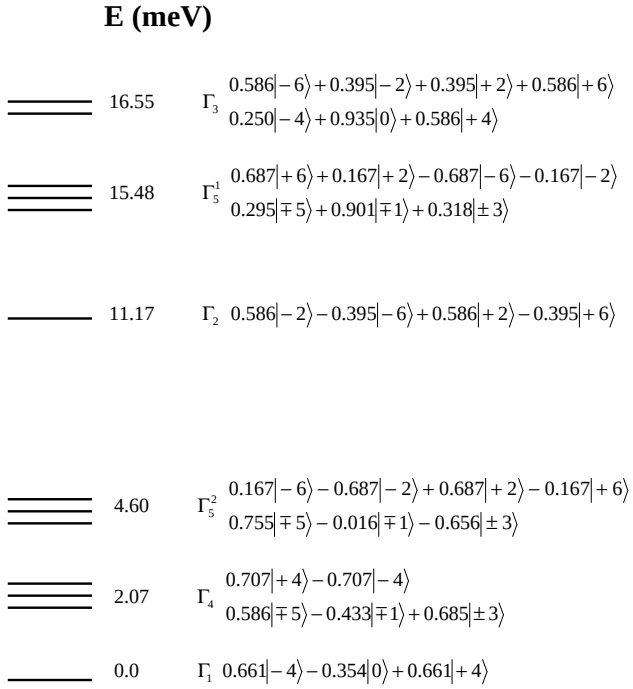

Figure 8. The crystal field level scheme for the $^7F_6$ state of Tb^{3+} in $TbNi_2$ and the corresponding wave functions are shown.

superstructure of the Laves phase, i.e. the calculation has been performed for the cubic Laves phase structure, and (ii) we neglect the small rhombohedral distortion below T_C.

The absence of resolvable peaks in the INS imposes a strong constraint on the values of the x parameter in the Lea–Leask–Wolf (LLW) diagram [15]: there is only the region at $x = -0.8$ suitable to fit the 40 K data. The solid lines in figure 7 are the results of a profile refinement of the CF model; the individual transitions are shown by the dashed lines. The values of the (LLW) CF parameters thus obtained in the paramagnetic range from the fit of the Hamiltonian for the fourfold axis using a Lorentzian line shape with $\Gamma = 1.77 \pm 0.03$ meV are: $x = -(0.871 \pm 0.001)$ and $W = -(0.076 \pm 0.001)$ meV; $B_4 = (1.11 \pm 0.02) \times 10^{-3}$ meV and $B_6 = -(1.3 \pm 0.02) \times 10^{-6}$ meV. The resulting level scheme is shown in figure 8 together with the corresponding wave functions.

The INS measured at 8 K shows that the ferromagnetic order changes the CF excitation spectrum significantly. For the fit of the data in the ordered state a Hamiltonian given by: $H = H_{cf}^{111} + H_{mf}$ was applied, where H_{cf}^{111} is the Hamiltonian for the threefold axis, taking into account the space diagonal [111] as the magnetization direction, since the Tb moments in their majority are aligned along the space diagonal:

$$H_{cf}^{111} = B_4^{0(3)}[O_4^0 - 20\sqrt{2}O_4^2]^{(3)} + B_6^{0(3)}[O_6^0 + (35\sqrt{2}/4)O_6^3 + \tfrac{77}{8}O_6^6]^{(3)}.$$

The relations of the CF parameters in this H_{cf}^{111} to those determined in the paramagnetic regime ($T = 40$ K) with the fourfold axis are: $B_4^{0(3)} = (-2/3)B_4$ and $B_6^{0(3)} = (16/9)B_6$ (see Hutchings' equation (6.15), [16].)

The molecular field Hamiltonian H_{mf} is the sum of two terms of the form $H_\alpha . J_\alpha$ with $\alpha = x$ and z. The fit revealed for the two parameters $H_X = -0.48 \pm 0.01$ meV and

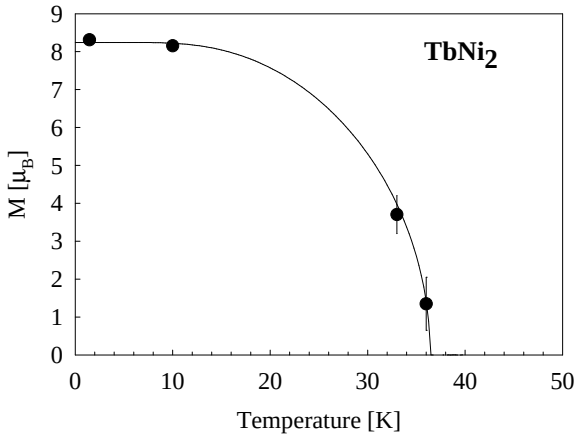

Figure 9. The calculated temperature dependence of the spontaneous magnetization is given by the solid line. The symbols indicate the data obtained from the FULLPROF analysis of the elastic diffraction spectra.

$H_z = 1.19 \pm 0.01$ meV and the magnetic moment obtained from this calculation is 8.27 μ_B/Tb being in good agreement with 8.3 μ_B/Tb determined from the diffraction pattern at 1.5 K. A common line-width Γ for the Lorentzian line shape was used for all the transitions at one temperature $\Gamma_{(8\ \mathrm{K})} = 1.46 \pm 0.02$ meV and $\Gamma_{(40\ \mathrm{K})} = 1.77 \pm 0.03$ MeV.

As can be seen from figure 7 the model used describes the measured $S(Q, \omega)$ function well at both temperatures. The non-vanishing value for the H_X parameter is related to the spin reorientation below 14 K where the Tb moments on Tb4 and Tb5 sites are perpendicular to the [111] direction.

Having determined the CF parameter, we calculated the temperature dependence of the spontaneous magnetization in the self-consistent mean field approximation using the threefold-axis CF Hamiltonian (given above). The molecular field parameter has been estimated from the Curie temperature, the resulting value $\lambda = 3.325$ mol emu^{-1}. The result of the calculation shown by the full line in figure 9 is in good agreement with the moments deduced from the FULLPROF analysis at several temperatures (full circle). Finally it should be noted that the level scheme and corresponding wavefunctions are not much different to these obtained by Goremychkin *et al* [17] on stoichiometric $TbNi_2$. As can be seen from figure 8 $TbNi_2$ is a system with a non-magnetic ground state level and consequently the magnetic order will be possible only when the exchange interaction is sufficiently strong to produce a mixing of the ground and the excited levels. Therefore the two triplets at 2 and 4.6 meV play a crucial role for the magnetic stability. As the temperature decreases below T_C both these triplets will be gradually depopulated and slightly split by the MF. This depopulation of the triplets with decreasing temperature in combination with the exchange interaction in the vicinity of the regular arranged vacancies is to our opinion responsible for the appearance of the spin reorientation at 14 K in the superstructure.

4. Conclusion

$TbNi_2$ crystallizes in a cubic structure which is a superstructure (space group F-43m) of the cubic Laves phase, characterized by a doubling of the Laves cell parameter and by regular arranged vacancies on the rare earth sites.

The anomaly at 14 K ($=T_R$) detected by AC-susceptibility, specific heat, magnetostriction and magnetoresistance measurements is associated with a spin reorientation on some of the Tb sites in the superstructure. Elastic neutron diffraction experiments revealed that [111] is the easy axis of magnetization for $T_R < T < T_C$ ($T_C = 36$ K), while below T_R the Tb moments on three of the eight non-equivalent Tb sites rotate out of the easy axis into a plane perpendicular to [111]. Inelastic neutron diffraction experiments have been employed to determine the crystal field level scheme. The calculation of the temperature dependence of the spontaneous magnetization using a combination of a crystal field and a molecular field Hamiltonian yields a good agreement with those determined by the FULLPROF analysis of the elastic neutron diffraction data. The spin reorientation at T_R is due to an interplay of the exchange interaction in the neighbourhood of the vacancies and the crystal field properties which yield a mixing of the ground state with the triplets at 2 and 4.6 meV and their depopulation as the temperature is reduced.

Acknowledgment

We thank ILL for beam time on the D1A (elastic neutron experiment). This project has been supported by the Austrian Science Foundation (FWF) under the projects P11581 PHY and S5605. This work was also supported by the US Department of Energy BES-MS under contract No W-31-109 ENG-38 (inelastic neutron diffraction). One of us, EG, wishes also to express thanks for the financial support from INTAS 96-0630.

References

[1] Felcher G P, Corliss L M and Hastings J M 1965 *J. Appl. Phys.* **36** 1001
[2] Latroche M, Paul-Boncour V, Percheron-Guegan A and Achard J C 1990 *J. Less-Common Met.* **161** L27
[3] Latroche M, Paul-Boncour V and Percheron-Guegan A 1993 *Z. Phys. Chem.* **179** 261
[4] Lindbaum A, Hafner J and Gratz E 1999 *J. Phys.: Condens. Matter* **11** 1177
[5] Gratz E *et al* 1996 *J. Phys.: Condens. Matter* **8** 8351
[6] Rodriguez-Carvajal J 1993 *Physica* B **192** 22
[7] Gratz E and Zuckermann M J 1982 *Handbook on the Physics and Chemistry of Rare Earths* vol 5, ed K A Gschneidner Jr and L Eyring (Amsterdam: North-Holland) ch 42, p 172
[8] Markosyan A S 1980 *Sov. Phys–Solid State* **22** 2023
[9] Markosyan A S 1999 private communication
[10] Bleany B 1963 *Proc. R. Soc.* A **276** 28
[11] Farrell J and Wallace W E 1966 *Inorg. Chem.* **5** 105
[12] Burzo E and Laforest J 1972 *Int. J. Magn.* **3** 171
[13] Ibarra M R del Moral A and Abell J S 1984 *J. Magn. Magn. Mater.* **46** 157
[14] Melero J J and Burriel R 1996 *J. Magn. Magn. Mater.* **157/158** 651
[15] Lea K R, Leask M J M and Wolf W P 1962 *J. Phys. Chem. Solids* **23** 1381
[16] Hutchings M T 1964 *Solid State Phys.* **16** 227
[17] Goremychkin E A, Natkaniec I, Mühle E and Chistyakov O D 1989 *J. Magn. Magn. Mater.* **81** 63